High-speed inline holographic Stokesmeter imaging

Xue Liu,[1] Alexander Heifetz,[1,3] Shih C. Tseng,[4] and M. S. Shahriar[1,2,*]

[1]Department of Electrical Engineering and Computer Science, Northwestern University, Evanston, Illinois 60208, USA

[2]Department of Physics and Astronomy, Northwestern University, Evanston, Illinois 60208, USA

[3]Nuclear Engineering Division, Argonne National Laboratory, Argonne, Illinois 60439, USA

[4]Digital Optical Technologies, Inc., Rolling Meadows, Illinois 60008, USA

*Corresponding author: shahriar@northwestern.edu

Received 13 February 2009; revised 22 May 2009; accepted 26 May 2009; posted 1 June 2009 (Doc. ID 107549); published 1 July 2009

We demonstrate a high-speed inline holographic Stokesmeter that consists of two liquid crystal retarders and a spectrally selective holographic grating. Explicit choices of angles of orientation for the components in the inline architecture are identified to yield higher measurement accuracy than the classical architecture. We show polarimetric images of an artificial scene produced by such a Stokesmeter, demonstrating the ability to identify an object not recognized by intensity-only imaging systems.

OCIS codes: 110.5405, 090.2890.

1. Introduction

Polarization imaging takes advantage of polarization-sensitive reflection of light from different media. It has been used for a variety of applications, including vegetation mapping, pollution monitoring, geological surveys, medical diagnostics, computer vision, and scene discrimination [1–5]. An arbitrary polarization state of light can be represented by the Stokes vector, which is defined in terms of transverse components E_x and E_y of the electric field:

$$\vec{S}(\tau) \equiv \begin{pmatrix} I \\ Q \\ U \\ V \end{pmatrix} \equiv \begin{pmatrix} \langle E_x E_x^* \rangle + \langle E_y E_y^* \rangle \\ \langle E_x E_x^* \rangle - \langle E_y E_y^* \rangle \\ \langle E_x E_y^* \rangle + \langle E_y E_x^* \rangle \\ i\langle E_x E_y^* \rangle - i\langle E_y E_x^* \rangle \end{pmatrix}, \quad (1)$$

where the brackets imply averaging over an observation time of τ. Here I is the overall intensity, Q denotes the intensity difference between vertical and horizontal linear polarizations, U represents the intensity difference between linear polarizations at $+45°$ and $-45°$, and V is the intensity difference between left and right circular polarizations. Measurement of the polarization state of the scattered light is often accomplished with a Stokesmeter that typically consists of several passive polarization-sensitive optical components and an intensity detector. A Mueller matrix is used to describe mathematically how the optical components of the Stokesmeter change the polarization state of the transmitted light [6,7]. The net Mueller matrix of the Stokesmeter is given by the ordered product of the Mueller matrices of the individual optical elements.

The classical Stokesmeter consists of a quarter-wave plate (QWP) and a linear polarizer (LP) [8] and requires the QWP to be inserted and removed between various readings. Consequently, the speed of the system is greatly limited. This problem can be circumvented by using a pair of liquid crystal retarders (LCRs) in series with a polarizer. Such an architecture, capable of high-speed inline Stokesmetry, has been investigated theoretically [9] as well as experimentally [10–12]. Here we describe and demonstrate a variation of this architecture in which the polarizer is replaced by a polarization-sensitive holographic grating. For a given wavelength of

0003-6935/09/193803-06$15.00/0

illumination, the holographic grating is essentially equivalent to the conventional polarizer. However, it has the added capability of spectral multiplexing. By tilting the angle of the grating, it is possible to select a narrow spectral band of the input light. Thus, in effect, this system can be used to combine spectrally multiplexed imaging with Stokesmetric imaging in high-speed inline architecture.

Previously, we demonstrated other types of holographic Stokesmeter [13–15]. However, the version demonstrated here is distinctly different from the previous versions. Specifically, there is no need to split the input beam into two parts in this architecture, thus making it much easier to perform Stokesmetric imaging. We demonstrate the ability of such a device to identify an object not recognizable through intensity-only imaging by analyzing the content of Stokesmetric images.

In Section 2 we briefly recall the operation of a classical Stokesmeter. In Section 3 we review the architecture of an inline Stokesmeter and identify parameters that optimize the accuracy. In Section 4 we describe a LCR-based Stokesmeter constructed with polarization-sensitive holographic gratings. In Section 5 we present the experimental results that verify the increased accuracy of the inline architecture for the condition identified in Section 3. In Section 6 we demonstrate polarimetric imaging of an artificial scene with the inline holographic Stokesmeter.

2. Classical Stokesmeter Architecture

The classical method to measure the Stokes parameters is illustrated in Fig. 1. It consists of a removable QWP and a rotating LP. The first three measurements of the transmitted intensity, denoted as I_1, I_2, and I_3, are carried out with the QWP removed, while the transmission axis of the LP is rotated clockwise (when looking in the direction of the beam propagation) to 0°, 90°, and 45°, respectively. I_4 denotes the measured intensity after inserting the QWP with the fast axis at 0° and the LP oriented at 45°. The system can be represented by

$$\vec{I} = A\vec{S}, \tag{2}$$

where $\vec{I} = [I_1, I_2, I_3, I_4]^T$, $\vec{S}$ is the input Stokes vector, and A is defined as the measurement matrix. The computed elements of A are given by

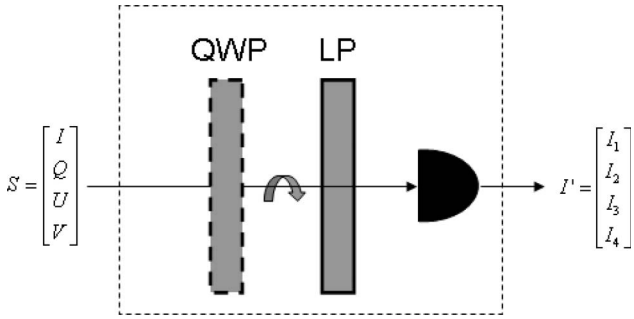

Fig. 1. Classical Stokesmeter with a removable QWP and a rotating LP.

$$A = \frac{1}{2}\begin{bmatrix} 1 & 1 & 0 & 0 \\ 1 & -1 & 0 & 0 \\ 1 & 0 & 1 & 0 \\ 1 & 0 & 0 & 1 \end{bmatrix}. \tag{3}$$

Stokes vector $\vec{S}$ is given by $\vec{S} = A^{-1}\vec{I}$.

3. Inline Stokesmeter

Figure 2 shows the inline Stokesmeter akin to what was presented by Ambirajan and Look [16]. In this architecture, the QWP and the LP are rotated simultaneously for each measurement, which allows for higher operational speed than the classical Stokesmeter because no removal or insertion of the QWP is required. For an input light beam with Stokes vectors $\vec{S} = [I, Q, U, V]^T$ transmitted through the QWP rotated at an angle β_i followed by the LP rotated at an angle α_i, the Stokes vector of output beam $\vec{S'} = [I', Q', U', V']^T$ is

$$\vec{S'} = M\vec{S}, \tag{4}$$

where $M = M_{\mathrm{LP}}M_{\mathrm{QWP}}$ equals the product of the Mueller matrices of the QWP and the LP [17]. Using the well-known Mueller matrices for a QWP and a LP, the following relation is obtained:

$$\begin{bmatrix} I' \\ Q' \\ U' \\ V' \end{bmatrix} = \frac{1}{2}\begin{bmatrix} 1 & \cos 2\beta_i \cos 2(\alpha_i - \beta_i) & \sin 2\beta_i \cos 2(\alpha_i - \beta_i) & \sin 2(\alpha_i - \beta_i) \\ \cos 2\alpha_i & \cos 2\alpha_i \cos 2\beta_i \cos 2(\alpha_i - \beta_i) & \cos 2\alpha_i \sin 2\beta_i \cos 2(\alpha_i - \beta_i) & \cos 2\alpha_i \sin 2(\alpha_i - \beta_i) \\ \sin 2\alpha_i & \sin 2\alpha_i \cos 2\beta_i \cos 2(\alpha_i - \beta_i) & \sin 2\alpha_i \sin 2\beta_i \cos 2(\alpha_i - \beta_i) & \sin 2\alpha \sin 2(\alpha_i - \beta_i) \\ 0 & 0 & 0 & 0 \end{bmatrix}\begin{bmatrix} I \\ Q \\ U \\ V \end{bmatrix}. \tag{5}$$

The intensity observed by detector I' is given by

$$I'(\alpha_i, \beta_i) = \frac{1}{2}[I + Q\cos 2\beta_i \cos 2(\alpha_i - \beta_i) + U \sin 2\beta_i \cos 2(\alpha_i - \beta_i) + V \sin 2(\alpha_i - \beta_i)]. \tag{6}$$

To determine the four Stokes parameters, four measurements of transmitted intensity I' are taken with different combinations of α_i and β_i, yielding the equation $\widehat{I} = A_{\mathrm{IL}}\widehat{S}$, where A_{IL} is the measurement matrix for this system given by

$$A_{\mathrm{IL}} = \frac{1}{2}\begin{bmatrix} 1 & \cos 2\beta_1 \cos 2(\alpha_1 - \beta_1) & \sin 2\beta_1 \cos 2(\alpha_1 - \beta_1) & \sin 2(\alpha_1 - \beta_1) \\ 1 & \cos 2\beta_2 \cos 2(\alpha_2 - \beta_2) & \sin 2\beta_2 \cos 2(\alpha_2 - \beta_2) & \sin 2(\alpha_2 - \beta_2) \\ 1 & \cos 2\beta_3 \cos 2(\alpha_3 - \beta_3) & \sin 2\beta_3 \cos 2(\alpha_3 - \beta_3) & \sin 2(\alpha_3 - \beta_3) \\ 1 & \cos 2\beta_4 \cos 2(\alpha_4 - \beta_4) & \sin 2\beta_4 \cos 2(\alpha_4 - \beta_4) & \sin 2(\alpha_4 - \beta_4) \end{bmatrix}. \tag{7}$$

The determinant of measurement matrix $|A_{\mathrm{IL}}|$ governs in part the accuracy of the measurement process. We have carried out a systematic tabulation of $|A_{\mathrm{IL}}|$ as a function of angles α_i and β_i and determined that $|A_{\mathrm{IL}}|_{\max} = 0.184$. Note that this value is larger than $|A| = 0.125$ for the conventional Stokesmeter. We found that more than one possible combination yields this maximum value of $|A_{\mathrm{IL}}|$, as shown in Table 1. Explicit choices of parameters in this form have not been reported previously, to the best of our knowledge.

The Stokesmeter described above can be realized with components that are rotated mechanically. Alternatively, it is possible to construct a system with two voltage-controlled LCRs along with a LP at a fixed orientation [15,16,18]. Free from any mechanical motion, this device can easily achieve the video-rate operation. Figure 3 shows the basic schematic diagram of such a Stokesmeter. The incident light propagates through LCR1 and LCR2 (fast axis rotated by $\frac{\pi}{8}$) followed by a LP with the transmission axis oriented at $\frac{\pi}{4}$. The Mueller matrix for this system is

$$\begin{aligned} M &= M_{\mathrm{LP}}\left(\frac{\pi}{4}\right) M_{\mathrm{LCR2}}\left(\phi_2, \frac{\pi}{8}\right) M_{\mathrm{LCR1}}(\phi_1) \\ &= \frac{1}{2}\begin{bmatrix} 1 & \frac{1}{2}(1-\cos\phi_2) & \frac{1}{2}\cos\phi(1+\cos\phi_2) - \frac{\sqrt{2}}{2}\sin\phi_1\sin\phi_2 & \frac{1}{2}\sin\phi(1+\cos\phi_2) + \frac{\sqrt{2}}{2}\cos\phi_1\sin\phi_2 \\ 0 & 0 & 0 & 0 \\ 1 & \frac{1}{2}(1-\cos\phi_2) & \frac{1}{2}\cos\phi(1+\cos\phi_2) - \frac{\sqrt{2}}{2}\sin\phi_1\sin\phi_2 & \frac{1}{2}\sin\phi(1+\cos\phi_2) + \frac{\sqrt{2}}{2}\cos\phi_1\sin\phi_2 \\ 0 & 0 & 0 & 0 \end{bmatrix}, \end{aligned} \tag{8}$$

where ϕ_1 and ϕ_2 denote the phase retardations produced by LCR1 and LCR2, respectively. In the first three measurements, ϕ_1 is set to 0, $\frac{\pi}{2}$, and π consecutively, whereas ϕ_2 is kept at 0. In the fourth measurement, the voltage on LCR2 is adjusted so that $\phi_2 = \pi$, whereas the phase retardation produced by LCR1 remains π. The measurement matrix for such a system, as calculated according to the first row of the Mueller matrix in Eq. (8), is found to be

$$A = \frac{1}{2}\begin{bmatrix} 1 & 0 & 1 & 0 \\ 1 & 0 & 0 & 1 \\ 1 & 0 & -1 & 0 \\ 1 & 1 & 0 & 0 \end{bmatrix}. \tag{9}$$

The determinant of the measurement matrix is $|A| = 0.125$ for the particular implementation shown in Eq. (9). We found that this is the highest determinant achievable with this architecture. With the LCR (from Meadowlark, Incorporated) used in our current setup, it takes approximately 20 ms to complete the full circle of four measurements, enabling it to be operated at a video-rate speed.

4. Inline, Spectrally Selective Holographic Stokesmeter

The architecture described in Fig. 3 makes use of a conventional polarizer. As an alternative, such a polarizer can be replaced by a holographic grating designed to work as a spectrally selective polarizer. This architecture is illustrated schematically in Fig. 4. To replace the LP oriented at 45° in the Stokesmeter demonstrated in Fig. 3, the hologram is written to have a polarization-selective diffraction efficiency η such that $\eta = \eta_0 \cos^2(\theta - \frac{\pi}{4})$, where θ is the angle of the input polarization with respect to the

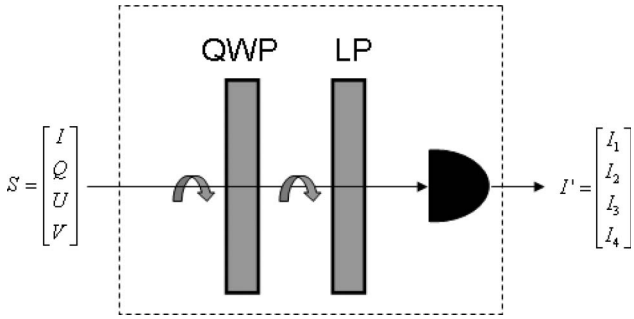

Fig. 2. Inline automatic Stokesmeter with a rotating QWP and a rotating LP.

Table 1. Four Sets of Combinations of QWP and LP Angles that Yield High $|A_{IL}|$ Values

α_1	β_1	α_2	β_2	α_3	β_3	α_4	β_4	$\lvert A_{IL}\rvert$
0°	60°	15°	0°	45°	45°	90°	15°	0.184
0°	60°	15°	0°	60°	60°	90°	15°	0.184
0°	75°	30°	30°	75°	90°	90°	30°	0.184
0°	75°	45°	45°	75°	90°	90°	30°	0.184

vertical axis with η_0 close to unity. Such a grating can easily be written, as discussed in Ref. [13]. As shown in Ref. [15], this grating is also spectrally selective. For a given angle of incidence, only light in a very narrow band ($\Delta\lambda \cong 1$ nm for a grating thickness of 1 mm) undergoes diffraction. Within this band, this device is then equivalent to the Stokesmeter discussed in Section 3. Furthermore, by tilting its angular orientation, we can select a different band of light. Therefore, such a Stokesmeter is able to perform high-speed spectrally multiplexed inline Stokesmetric imaging.

5. Measuring the Stokes Vector

In Section 3 we identified optimum operating conditions for the inline Stokesmeter for both the mechanical and the LCR-based versions. To test the validity of these parameters, we carried out measurement of the Stokes parameters using an inline Stokesmeter

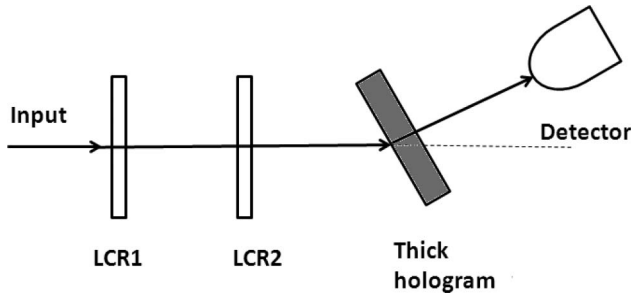

Fig. 4. Schematic diagram of the inline, spectrally selective holographic Stokesmeter.

and compared the results with those obtained using classical architecture. For both architectures, we studied three different polarization states of light: (a) linear −45° polarized light, (b) linear horizontally polarized light, and (c) right circularly polarized light. As shown in Fig. 5, compared with the measurement made by the classical Stokesmeter, the Stokes parameters measured by the inline architecture are closer to the theoretical value for all three cases. We define the accuracy of the measurement as follows:

$$\varepsilon = \left(1 - \left|\frac{S_{\text{meas}} - S_{\text{theo}}}{I_{\text{theo}}}\right|\right) \times 100\%, \qquad (10)$$

where S_{meas} and S_{theo} stand for measured and theoretical values of Stokes parameters (I, Q, U, and V). I_{theo} stands for the theoretical value of the intensity that is normalized to unity in our calculation. The average accuracy of the measurements done by the inline Stokesmeter is improved from 94.14% of the conventional method to 98.85%, whereas the system error remains nearly unchanged (approximately 0.8%). The possible sources of this residual error include the imperfection of the HWP and the LP, the imprecision in orienting the optical components, and the inherent intensity noise in the detection process.

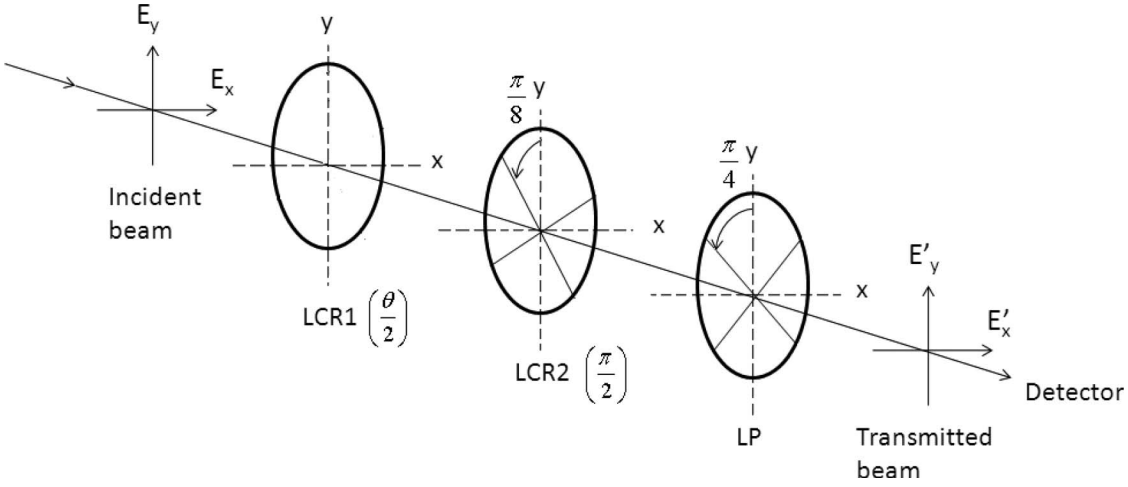

Fig. 3. High-speed inline Stokesmeter with two LCRs and a LP.

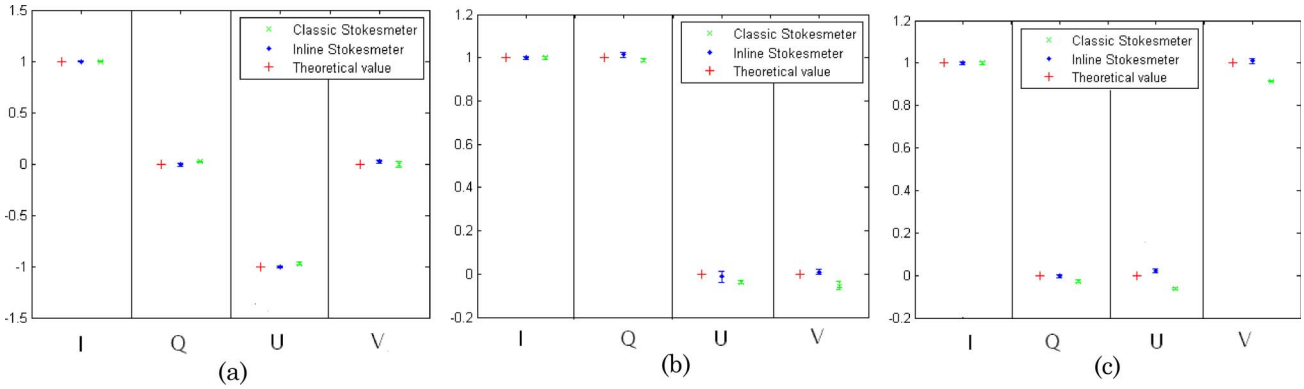

Fig. 5. (Color online) Comparison of the Stokes parameters measured by the inline Stokesmeter and the classic Stokesmeter: (a) linear −45° polarized light, (b) linear horizontally polarized light, (c) right circularly polarized light.

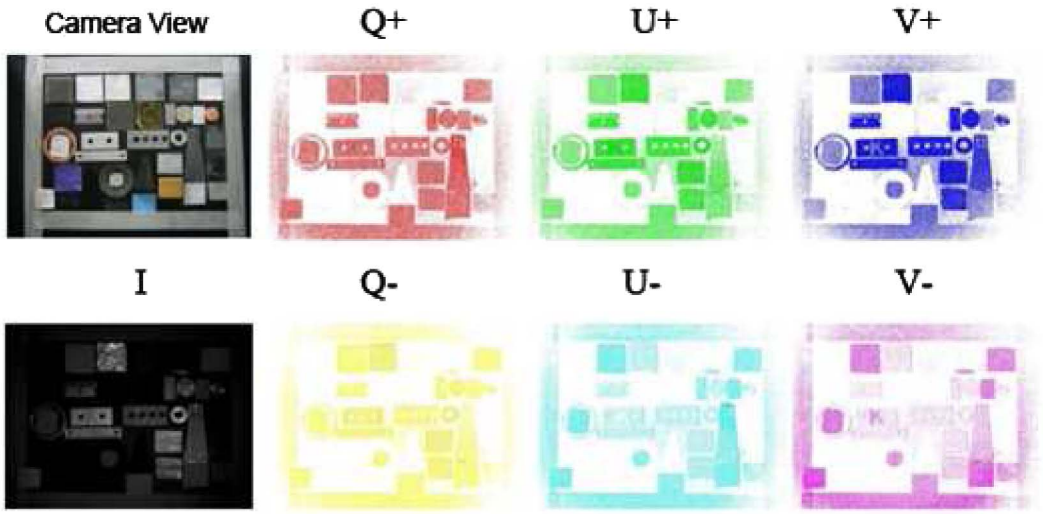

Fig. 6. (Color online) Polarization imaging for a set of objects with various polarization properties. The objects are illuminated by left circularly polarized light.

6. Polarization Imaging with the Inline Holographic Stokesmeter

We used the inline automatic holographic Stokesmeter illustrated in Fig. 4 to analyze the polarization images for an artificial scene. The tested objects of different polarimetric properties include leaves, sandpaper, and different types of metal. We purposely attached a transparent adhesive tape to one piece of metal in the center of the scene to form the shape of the letter K. The objects were illuminated by left circularly polarized light. The reflection is analyzed by the inline holographic Stokesmeter. Since the attached tape does not change the reflectivity of the metal significantly, it cannot be easily identified in the camera view as shown in the first frame of Fig. 6. However, when the Stokes vector of light reflected by the scene is analyzed by the inline Stokesmeter from the images that contain only the left and right circularly polarized light (V_-/V_+), the letter K shaped by the tape can be easily identified in the complex scenery that is due to the different polarimetric properties of the tape and the surroundings.

7. Conclusion

To summarize, we have presented an inline holographic Stokesmeter consisting of two liquid crystal retarders and a spectrally selective holographic grating capable of operation at the video-frame rate. We also identified explicit choices of angles of orientation for the components in the inline architecture to yield higher accuracy of measurements than the classical architecture. The polarimetric images of an artificial scene produced by such a Stokesmeter show the ability to identify an object indiscernible by conventional intensity imaging systems.

This research is supported in part by United States Air Force Office of Scientific Research (USAFOSR) grant FA9550-06-1-04, Office of Naval Research (ONR) contract N00014-07-M-0173, and Department of Energy (DOE) grant DE-AC02-06CH11357.

Reference

1. L. J. Denes, M. Gottlieb, B. Kaminsky, and D. Huber, "Spectropolarimetric imaging for object recognition," Proc. SPIE **3240**, 8–18 (1998).

2. T. Nee and S. F. Nee, "Infrared polarization signatures for targets," Proc. SPIE **2469**, 231–241 (1995).
3. P. J. Curran, "Polarized visible light as an aid to vegetation classification," Remote Sens. Environ. **12**, 491–499 (1982).
4. L. D. Travis, "Remote sensing of aerosols with the earth-observing scanning polarimeter," Proc. SPIE **1747**, 154–164 (1992).
5. M. J. Duggin, "Imaging polarimetry in scene element discrimination," Proc. SPIE **3754**, 108–117 (1999).
6. S.-Y. Lu and R. A. Chipman, "Interpretation of Mueller matrices based on polar decomposition," J. Opt. Soc. Am. A **13**, 1106–1113 (1996).
7. J. S. Baba, J.-R. Chung, A. H. DeLaughter, B. D. Cameron, and G. L. Cote, "Development and calibration of an automated Mueller matrix polarization imaging system," J. Biomed. Opt. **7**, 341–349 (2002).
8. D. Goldstein, *Polarized Light*, 2nd ed. (CRC Press, 2003).
9. J. M. Bueno, "Polarimetry using liquid-crystal variable retarders: theory and calibration," J. Opt. A Pure Appl. Opt. **2**, 216–222 (2000).
10. A. De Martino, E. Garcia-Caurel, B. Laude, and B. Drévillon, "Optimized Mueller polarimeter with liquid crystals," Opt. Lett. **28**, 616–618 (2003).
11. B. Laude-Boulesteix, A. De Martino, B. Drévillon, and L. Schwartz, "Mueller polarimetric imaging system with liquid crystals," Appl. Opt. **43**, 2824–2832 (2004).
12. F. Goudail, P. Terrier, Y. Takakura, L. Bigué, F. Galland, and V. DeVlaminck, "Target detection with a liquid-crystal-based passive Stokes polarimeter," Appl. Opt. **43**, 274–282 (2004).
13. M. S. Shahriar, J. T. Shen, R. Tripathi, M. Kleinschmit, T.-W. Nee, and S.-M. F. Nee, "Ultrafast holographic Stokesmeter for polarization imaging in real time," Opt. Lett. **29**, 298–300 (2004).
14. J.-K. Lee, J. T. Shen, and M. S. Shahriar, "Demonstration of a spectrally scanned holographic Stokesmeter," Opt. Commun. **277**, 63–66 (2007).
15. T.-W. Nee, S.-M. F. Nee, M. W. Kleinschmit, and M. S. Shahriar, "Polarization of holographic grating diffraction. II. Experiment," J. Opt. Soc. Am. A **21**, 532–539 (2004).
16. A. Ambirajan and D. C. Look, Jr., "Optimum angles for a polarimeter: part I," Opt. Eng. **34**, 1651–1655 (1995).
17. E. Collett, *Polarized Light: Fundamentals and Applications* (Marcel Dekker, 1993).
18. A. Ambirajan and D. C. Look, Jr., "Optimum angles for a polarimeter: part II," Opt. Eng. **34**, 1656–1659 (1995).